Ligand-to-Metal Charge Transfer of Ag(II) CF_2X Carboxylates: Quantum Yield and Electrophotocatalytic Arene Fluoroalkylation Tuned by X

Brandon M. Campbell,† Jesse B. Gordon,† Elaine Reichert Raguram,† Kristopher G. Reynolds, Meghan G. Sullivan, and Daniel G. Nocera*

Abstract: Incorporation of CF_2X groups beyond CF_3 into arene scaffolds is underdeveloped despite these groups' utility as halogen-bond donors and as precursors to bioisosteres. Herein, we report the synthesis, characterization, and comparative photochemistry of a suite of $[Ag(II)(bpy)_2O_2CCF_2X]^+$ and $Ag(II)(bpy)(O_2CCF_2X)_2$ (bpy = 2,2′-bipyridine, X = F, CF_3, Cl, Br, H, CH_3) carboxylate complexes. We find a dramatic effect of the X substituent on the efficiency of generating CF_2X radicals by ligand-to-metal charge transfer (LMCT), with Ag(II) photoreduction rates varying by over an order of magnitude and quantum yields spanning over 20%. We provide insight into how electronic and structural perturbations of the $Ag(II)–O_2CCF_2X$ core are manifested in the LMCT quantum efficiency. With this information in hand, Ag(II)-mediated electrophotocatalytic CF_2X functionalization is carried out on a range of (hetero)arenes. This work expands the nascent field of Ag(II)-based photocatalysis by allowing for (hetero)aryl–CF_2X functionalization directly from unactivated fluoroalkyl carboxylate precursors.

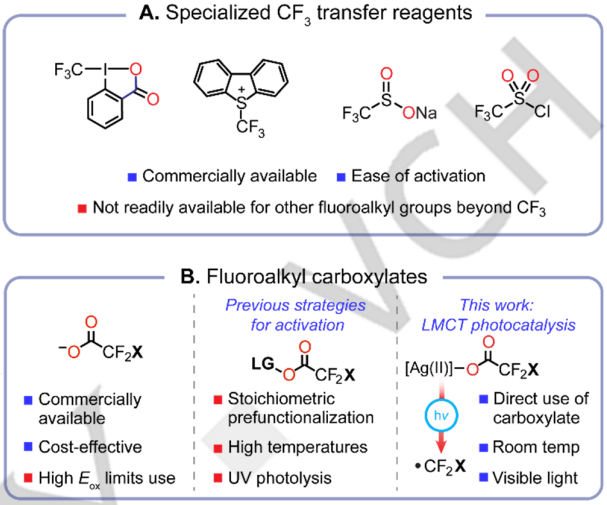

Figure 1. (**A**) Selected examples of common trifluoromethyl group transfer reagents. (**B**) Fluoroalkyl carboxylates as CF_2X group transfer reagents.

Introduction

The established benefits of fluorine incorporation into pharmaceuticals[1,2] have given rise to a variety of strategies to install fluorine into organic molecules. Fluoroalkyl groups feature prominently in FDA-approved pharmaceuticals, with the trifluoromethyl group (CF_3) being among the most prevalent.[3] Synthetic efforts to incorporate CF_3 groups benefit from the wide availability and well-described reactivity of specialty CF_3 group transfer reagents (**Figure 1A**).[4–6] Conversely, fluoroalkyl groups other than CF_3 are less common despite their beneficial properties. For example, CF_2X moieties (X = Cl, Br) can serve as $C(sp^3)$–X halogen bond donors, providing key binding interactions between small molecules and protein targets.[7] Beyond their utility as functional groups themselves, CF_2X groups can serve as precursors for further elaboration. They can be reduced to CF_2H groups,[8,9] which are lipophilic hydrogen-bond donors that can act as alcohol or thiol bioisosteres,[10] or undergo substitution, cross-coupling, or other C–C bond-forming reactions[11] to furnish R–CF_2–R′ moieties, which can behave as carbonyl bioisosteres.

An impediment to installing fluoroalkyl substituents beyond CF_3 into organic molecules arises from a dearth of accessible CF_2X reagents, which either do not exist or require multi-step syntheses to prepare. Current methods for synthesizing aryl–CF_2X[12–19] or (hetero)aryl–CF_2X[20–23] functionalized arenes often require pre-installation of an aryl–CX_3 or acyclic CF_2X-functionalized precursor, respectively. The necessity of prefunctionalization in these methods impedes the determination of structure-activity relationships in medicinal chemistry contexts, as each CX_3- or acyclic CF_2X-functionalized precursor must be synthesized individually, in contrast to a diversity-oriented approach in which a single precursor is poised to form several products of interest. More efficient methods that utilize •CF_2X to directly convert aryl–H to aryl–CF_2X are less common.[9,24–26]

An ideal source of CF_2X groups is their corresponding carboxylates (**Figure 1B**, left panel), due to their wide availability, low cost, and bench stability. However, the inertness of fluoroalkyl carboxylates, and the consequently harsh conditions required for their oxidation and subsequent decarboxylation, are impediments for their use in synthesis. For example, direct electrochemical oxidation of trifluoroacetate (TFA) requires high anodic potentials (E_{ox} > 2

Department of Chemistry and Chemical Biology
Harvard University
12 Oxford Street, Cambridge, MA 02138
E-mail: dnocera@fas.harvard.edu

[†] These authors contributed equally

Supporting information for this article is given via a link at the end of the document.

V vs SCE) approaching the redox stability windows of common solvents, as well as that of inert arenes such as benzene.[27,28] To bring the redox activation of fluoroalkyl carboxylates within a workable potential range, the few reported methods for the generation of $•CF_2X$ from fluoroalkyl carboxylate precursors tend to require stoichiometric prefunctionalization of the carboxylate (**Figure 1B**, middle panel).[9,24–26] As an alternative strategy, photoredox methods can provide access to the extreme redox potentials needed to furnish radicals directly from the carboxylates under overall mild conditions.[29–32,33] One such method is ligand-to-metal charge transfer (LMCT) photochemistry which uses light as an energy input to access a LMCT excited-state of an M^n–L complex, allowing for eventual dissociation of a ligand radical, •L, and concomitant formation of a reduced metal center, M^{n-1}. LMCT photochemistry has been employed to generate a range of radicals from various mid/high-valent metal centers, such as Cu(II),[34–36] Fe(III),[37,38] Ce(IV),[39] Ni(III/II),[40,41] and V(V).[42]

We have recently demonstrated the ability of Ag(II) to catalytically oxidize TFA *via* LMCT photochemistry.[29] In contrast to Fe(III)-based methods,[30,31,33,43] Ag(II) LMCT decarboxylation proceeds with visible light ($\lambda \geq 440$ nm) at high quantum efficiencies from isolable, well-defined, carboxylate-bound chromophores. The ability to push LMCT photochemistry into the visible spectral region at high quantum efficiencies is important to the sustainability footprint of a photoredox method,[44,45] as well as the facility for the method's practical scale-up.[46] For LMCT decarboxylations at a Ag(II) center, the highly oxidizing Ag(II) ion possesses extremely low-lying metal-centered acceptor orbitals (**Figure 2A**), allowing for facile transfer of electron density from carboxylate ligands to the metal using lower energy visible light rather than the higher energy UV or near-UV excitation typically necessary for LMCT reactivity. Given our ability to prepare well-defined Ag(II) TFA complexes that are active catalysts for (hetero)arene trifluoromethylation reactions, we sought to generate a wider array of CF_2X radicals from an expanded palette of Ag(II) CF_2X carboxylate complexes (**Figure 1B**, right panel). This would not only afford access to fluoroalkylations reactions beyond CF_3 incorporation, but would also allow for LMCT structure-function relationships to be examined. Specifically, we explore the dependence of ligand/metal redox potential on the efficiency of LMCT photochemistry involving metal–ligand bond homolysis, which to date has remains ill-defined.

We now report a suite of well-defined Ag(II) CF_2X (X = F, CF_3, Cl, Br, H, CH_3) carboxylates and determine how the LMCT quantum efficiency of carboxylate bond homolysis is altered as the electronic structure of the Ag(II)-O_2CCF_2X core is perturbed by X (**Figure 2B**). Building on our understanding of the photochemistry of Ag(II) fluoroalkyl carboxylates, we further develop a general electrophotocatalytic method to induce the chlorodifluoromethylation of a wide array of arenes,

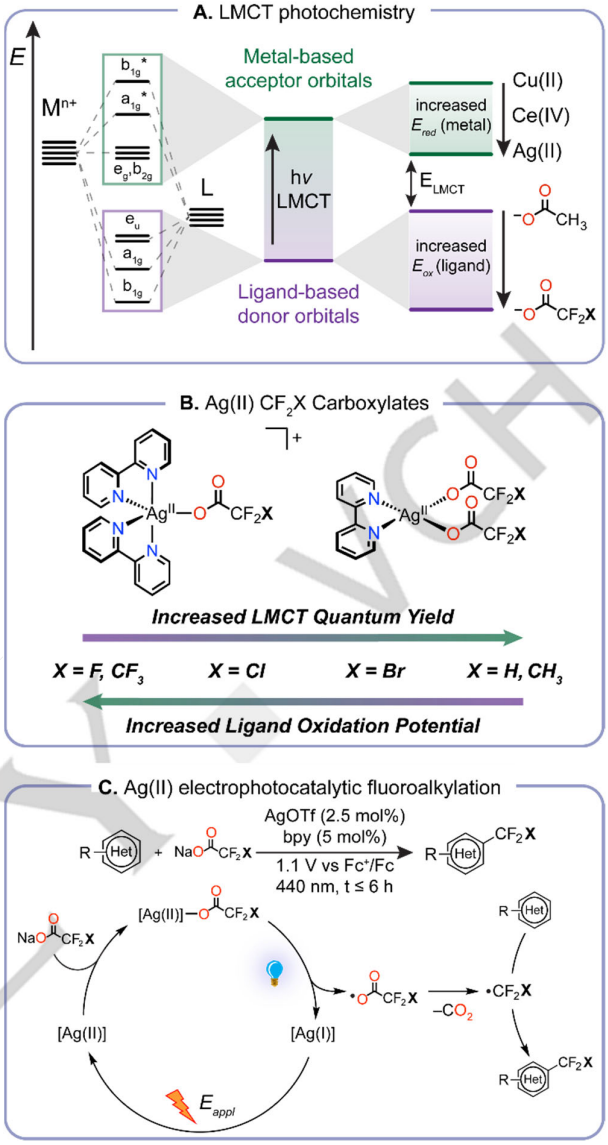

Figure 2. (**A**) Schematic of LMCT photochemistry: a simplified molecular orbital diagram (metal s and p orbitals not shown, σ-bonding only) for a generic D_{4h} metal complex is shown with an LMCT transition indicated by excitation of an electron in a ligand-centered orbital to a metal-centered orbital. The energies of these orbitals are correlated to the oxidation potential of the ligand and the reduction potential of the metal. (**B**) The Ag(II) CF_2X carboxylate complexes responsible for fluoroalkylation reactivity exhibit an inverse correlation between LMCT quantum yield and ligand oxidation potential. (**C**) This work: electrophotocatalytic fluoroalkylation using a Ag catalyst with inexpensive and abundant fluoroalkyl carboxylates.

including both five- and six-membered heteroarenes, as well as the bromodifluoromethylation and difluoroethylation of a narrower scope of simple arenes or electron-deficient heteroarenes, respectively (**Figure 2C**). This method simplifies the installation of these underutilized but useful functional groups by directly converting aryl–H to aryl–CF_2X using widely available carboxylates as the CF_2X source,

without the need for pre-activation of the arene or the carboxylate. In particular, this method provides convenient access to •CF_2Br, enabling the direct synthesis of aryl–CF_2Br from aryl–H, a transformation for which general methods did not previously exist. Ultimately, the results shown here add to a growing body of electrophotocatalytic decarboxylative radical transformations,[47–49] and furthermore demonstrate the synthetic utility of Ag(II) LMCT photochemistry as a general platform for radical generation from redox-reticent substrates.

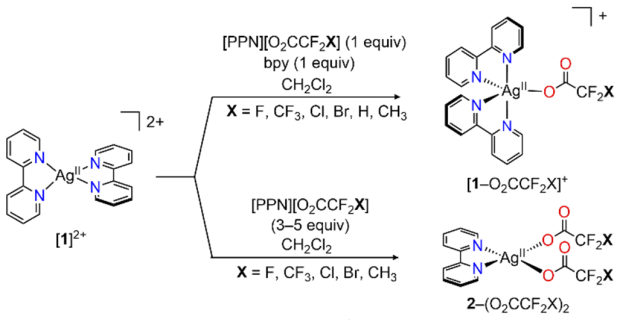

Scheme 1. Synthesis of Ag(II) carboxylate complexes.

Results and Discussion

Synthesis and characterization of Ag(II) CF_2X carboxylates

Although Ag(II) complexes are rare,[50] we recently developed a high-yielding procedure to prepare highly oxidizing, bench-stable, and organic-solvent-soluble $[Ag(bpy)_2]^{2+}$ (bpy = 2,2´-bipyridine) complexes.[29] The $[Ag(bpy)_2][OTf]_2$ (**1**$[OTf]_2$) complex serves as a starting reagent for synthesis of Ag(II)-bound carboxylate compounds. Binding of each carboxylate to $[\mathbf{1}]^{2+}$ was assessed through titration experiments monitored by UV-visible absorption spectroscopy. The titration of bis(triphenylphosphine)iminium (PPN) fluoroalkyl carboxylate salts to solutions containing **1**$[OTf]_2$ led to significant UV-vis spectral evolutions consistent with carboxylate binding to the Ag(II) center (**Figures S21–S23**). While evidence for the formation of multiple Ag(II)–O_2CCF_2X complexes can be seen in the titration data for X = Cl, Br, and CH_3, the carboxylate binding appeared to be weaker (and cation dependent) for X = H (**Figure S24**). On a preparative scale, complexes [**1**–O_2CCF_2X][OTf] and **2**–$(O_2CCF_2X)_2$ were obtained by the two general routes shown in **Scheme 1**. Treatment of **1**$[OTf]_2$ in dichloromethane (CH_2Cl_2) with the appropriate $[PPN][O_2CCF_2X]$ salt (1 equiv) in the presence of bpy (1 equiv) led to the formation of [**1**–O_2CCF_2X][OTf] (X = Cl, Br, H, CH_3), which could be crystallized as black needles upon vapor diffusion of pentane at –35 °C. Alternatively, treatment of **1**$[OTf]_2$ in CH_2Cl_2 with excess $[PPN][O_2CCF_2X]$ (3–5 equiv) followed by addition of pentane led to the precipitation of **2**–$(O_2CCF_2X)_2$ (X = Cl, Br, CH_3) as microcrystalline orange powders. Conversely, for X = H, even in the presence of excess carboxylate, only [**1**–O_2CCF_2H][OTf] could be isolated, consistent with the observed titration data. With the exception of **2**–$(O_2CCF_2CH_3)_2$, which is unstable in solution and crystallized as a mixture containing decomposition products, each complex could be isolated as an analytically pure solid. We previously reported the syntheses of the [**1**–O_2CCF_3][OTf] and **2**–$(O_2CCF_3)_2$ complexes, which are employed in this work as points of comparison against the new Ag(II) CF_2X (X = Cl, Br, H, and CH_3) carboxylate complexes.[29] While attempts to synthesize [**1**–$O_2CCF_2CF_3$][OTf] were unsuccessful, its synthesis as the tetrafluoroborate salt ([**1**–$O_2CCF_2CF_3$][BF_4] is accomplished here starting from **1**$[BF_4]_2$ via the route shown in **Scheme 1.** Attempts to synthesize [**1**–O_2CCF_2I][OTf] were unsuccessful, as treatment of **1**$[OTf]_2$ with [Na][O_2CCF_2I] or $[PPN][O_2CCF_2I]$ resulted in decomposition of **1**$[OTf]_2$ and formation of precipitates. Among the decomposition products, a Ag(I) iodide complex was identified (**Figure S11**).

Single-crystal X-ray diffraction analysis[51] of the [**1**–$O_2CCF_2X]^+$ series confirms their five-coordinate structure (**Figures 3A–3D** and **S1–S5**, **Tables S1** and **S2**). Inspection of the primary coordination sphere of each complex reveals a coordination geometry best described as intermediate between trigonal bipyramidal and square pyramidal ($0.45 < \tau_5 < 0.71$).[52] The Ag–O1 bond distances are all characteristically long (2.25–2.43 Å), similar to the previously reported [**1**–O_2CCF_3][OTf] (2.4814(15) Å). The carboxylate ligands assume a κ_1 binding mode, with secondary Ag–O1 interactions that exceed 2.8 Å. As the X group becomes more electronegative, the carboxylate becomes a weaker donor ligand, and accordingly *d*(Ag–O1) in the [**1**–O_2CCF_2X][OTf] complexes generally increases along the series X = CH_3 < Br < Cl < CF_3 < F (**Figure S6**); however, [**1**–O_2CCF_2H][OTf] displays a longer than expected d(Ag–O1) of 2.363(2) Å. Inspection of the crystallographic environment around the difluoromethyl carboxylate ligand reveals hydrogen bonding interactions between the CF_2–H unit and nearby oxygen atoms of the triflate counterions (**Figure S7**), which plausibly contribute to the increased distance of the carboxylate from the Ag center. In general, the long Ag(II)–carboxylate bonds across the series of complexes suggest weak interactions that are likely substantially influenced by crystal packing effects. This is evidenced by the observation of two crystallographically distinct molecules in the asymmetric unit of the crystal structure of [**1**–O_2CCF_2Br][OTf] with d(Ag–O1) values that differ by 0.101(3) Å (**Figure S3**).[53] Single-crystal X-ray diffraction analysis of **2**–(O_2CCF_2X) (X = Cl, Br, CH_3) (**Figures 3E–3F** and **S8–S10**) confirms their four-coordinate square planar nature ($0.09 < \tau_4 < 0.12$). [54] The asymmetric units of **2**–(O_2CCF_2X) feature tight Ag–O bonding interactions d(Ag–O1) and d(Ag–O3) that range between 2.14–2.16 Å. The **2**–$(O_2CCF_2X)_2$ complexes pack as inversion-symmetric dimers

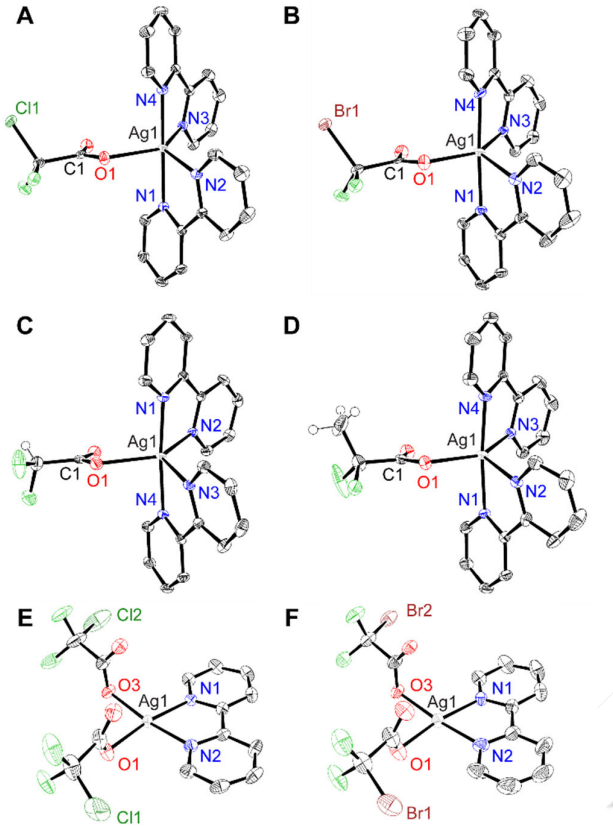

Figure 3. Solid-state structures of (**A**) [**1**–O_2CCF_2Cl][OTf], (**B**) [**1**–O_2CCF_2Br][OTf], (**C**) [**1**–O_2CCF_2H][OTf], (**D**) [**1**–$O_2CCF_2CH_3$][OTf], (**E**) **2**–$(O_2CCF_2Cl)_2$, and (**F**) **2**–$(O_2CCF_2Br)_2$ as ascertained by single-crystal X-ray diffraction analysis. Atomic displacement parameters drawn at 50% probability level. Ag, light gray; Br, maroon; Cl, dark green; F, light green; O, red; N, blue. Hydrogen atoms shown as white spheres. Counterions, solvent molecules, and hydrogen atoms on bpy ligands are omitted for clarity.

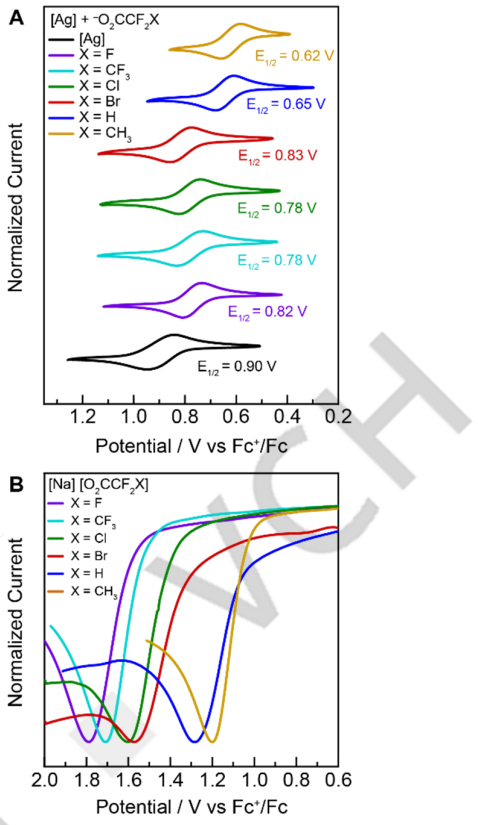

Figure 4. (**A**) Cyclic voltammograms for in situ generated $[Ag(bpy)_2]^+$ ([Ag] = 1 mM) and Ag(bpy)(O_2CCF_2X) complexes. (**B**) Linear sweep voltammograms for 2 mM [Na][O_2CCF_2X] (X = F, CF_3, Cl, Br, H, CH_3). Working electrode, glassy carbon; counter electrode, Pt wire; reference electrode, Ag/AgCl; scan rate: 100 mV s^{-1}; supporting electrolyte, $^nBu_4NPF_6$ (0.15 M).

in the solid-state, similar to the previously reported **2**–$(O_2CCF_3)_2$.

The stabilities of complexes [**1**–O_2CCF_2X]$^+$ and **2**–$(O_2CCF_2X)_2$ in solution are dramatically affected by the identity of the bound carboxylate. While [**1**–O2CCF$_2$X]$^+$ (X = F, CF_3, Cl) are relatively stable in acetonitrile (CH_3CN) solutions at room temperature over 12 h, as observed by UV-vis spectroscopy, [**1**–O_2CCF_2X]$^+$ (X = H, CH_3, Br) decay much more rapidly with observed rate constants increasing from Br < H < CH_3 (**Figure S25A**). The stability of these complexes improves significantly at 10 °C (**Figure S25B**). Complexes **2**–$(O_2CCF_2X)_2$ are less stable than their five-coordinate counterparts. The UV-vis-NIR features of **2**–$(O_2CCF_3)_2$ degrade by ca. 30% over 12 h, whereas **2**–$(O_2CCF_2Cl)_2$ and **2**–$(O_2CCF_2Br)_2$ completely decompose over the same time frame (**Figure S26**). This lack of stability for the Ag(II) CF_2X carboxylate complexes for X = Br, H, or CH_3 could be a potential factor in the diminished electrophotocatalytic reactivity observed for these carboxylates (vide infra).

To investigate potential causes of the decreased stability of the complexes when moving from X = F to X = CH_3, we undertook a series of electrochemical measurements. The presence of CF_2X carboxylates in the primary coordination sphere of **1**[OTf]$_2$ substantially alters the electrochemical properties of the complex (**Figure 4A**). Complex **1**[OTf]$_2$ displays a single, reversible Ag^{2+}/Ag^+ couple at ca. 900 mV vs Fc^+/Fc (Fc = ferrocene, all potentials hereafter are vs Fc^+/Fc), showcasing the powerful oxidizing nature of Ag(II). The perturbation of the redox couple by the fluoroalkyl carboxylate was assessed by recording the cyclic voltammogram of in situ generated $[Ag(bpy)_2]^+$ (from a mixture of AgOTf and bpy) with titration of the fluoroalkyl carboxylate. A gradual cathodic shift of the Ag^{2+}/Ag^+ couple is observed with increasing carboxylate equivalents (**Figures S28–S33**) until the invariant cyclic voltammogram shown in **Figure 4A** is attained. Furthermore, the cyclic voltammograms of the isolated [**1**–O_2CCF_3]$^+$ and **2**–$(O_2CCF_3)_2$ complexes exhibit redox waves that fall intermediate between those of the parent [**1**]$^{2+}$ complex and those observed in the presence of excess carboxylate (**Figure S34**). These observations are consistent with weak and fluxional binding of each carboxylate. The Randles-Ševčík

plots establish an electrochemically reversible couple (**Figures S35**–**S39**). The largest cathodic shift is observed for the more electron-rich carboxylates, $^{-}O_2CCF_2H$ and $^{-}O_2CCF_2CH_3$, indicating stronger donation into the Ag(II) center by these carboxylates, thereby quenching the metal ion's electrophilicity. To explore ground-state oxidation as a potential reason for instability, linear sweep voltammograms (LSVs) for the sodium salts of each carboxylate were measured **Figure 4B**. The peak oxidation potentials of the carboxylates occur at significantly more anodic potentials than that of **1**$[OTf]_2$, thus opening a redox window for the design of an electrophotocatalytic decarboxylation cycle (*vide infra*).

The [**1**–$O_2CCF_2X]^+$ complexes exhibit nearly identical absorption features (**Figure S27**), namely, a broad shoulder at 450 nm (ε_{450} = 1210–1560 M^{-1} cm^{-1}) and a weakly absorbing *d*-*d* transition at 700 nm (ε_{700} = 100–200 M^{-1} cm^{-1}). The corresponding **2**–$(O_2CCF_2X)_2$ complexes are weaker absorbers at 450 nm (ε_{450} = 990–1050 M^{-1} cm^{-1}) and lack the 700 nm absorption band that is characteristic of the five-coordinate [**1**–$O_2CCF_2X]^+$ complexes. LMCT absorption features are expected to correlate with the difference in redox potential of the ligand and metal.[55] However, we do not observe this correlation, despite the carboxylate redox potentials spanning a 500 mV range. The nearly identical absorption energies for [**1**–$O_2CCF_2X]^+$ suggest with a weaker, ionic association of the carboxylate with Ag(II), consistent with the longer carboxylate Ag(II) distances observed in the solid state. While little variation is seen in the electronic absorption spectra across the series of compounds, dramatic changes are observed in their LMCT photochemistry (*vide infra*).

LMCT photochemistry

With confirmation that the well-defined Ag(II) CF_2X carboxylate complexes are formed across the series of X substituents, we sought to examine their photolytic activity. Changes in the solution-state FT-IR spectra upon the irradiation of [**1**–O_2CCF_2X][OTf] with visible light (**Figure S40**) are consistent with the LMCT photoreaction shown in **Figure 5A**. Asymmetric and symmetric carboxyl stretches at 1685 and 1360 cm^{-1}, respectively, of [**1**–O_2CCF_2Cl][OTf] in CD_3CN gradually disappear with irradiation, and a new peak prominently appears at 2341 cm^{-1}, which is attributed to CO_2 (**Figure 5B**).[56] Taken together, the FT-IR data for photolyzed [**1**–O_2CCF_2Cl][OTf] solutions support the decarboxylation of $^{-}O_2CCF_2Cl$ to release CO_2 and $\bullet CF_2Cl$ upon LMCT excitation. The FT-IR spectra of the remaining complexes in the [**1**–$O_2CCF_2X]^+$ series show similar changes upon steady-state photolysis (**Figures S41–S44**). FT-IR difference spectra of the [**1**–$O_2CCF_2X]^+$ complexes are compared in **Figure 5C**. Whereas relatively small growth of higher frequency signals (1700–1900 cm^{-1}) are observed for [**1**–$O_2CCF_2X]^+$ (X = CF_3, Cl, Br, and CH_3), a large, sharp signal appears at 1756 cm^{-1} during photolysis of the X = H complex. This stretch is attributed to difluoroacetic acid (HO_2CCF_2H), which suggests

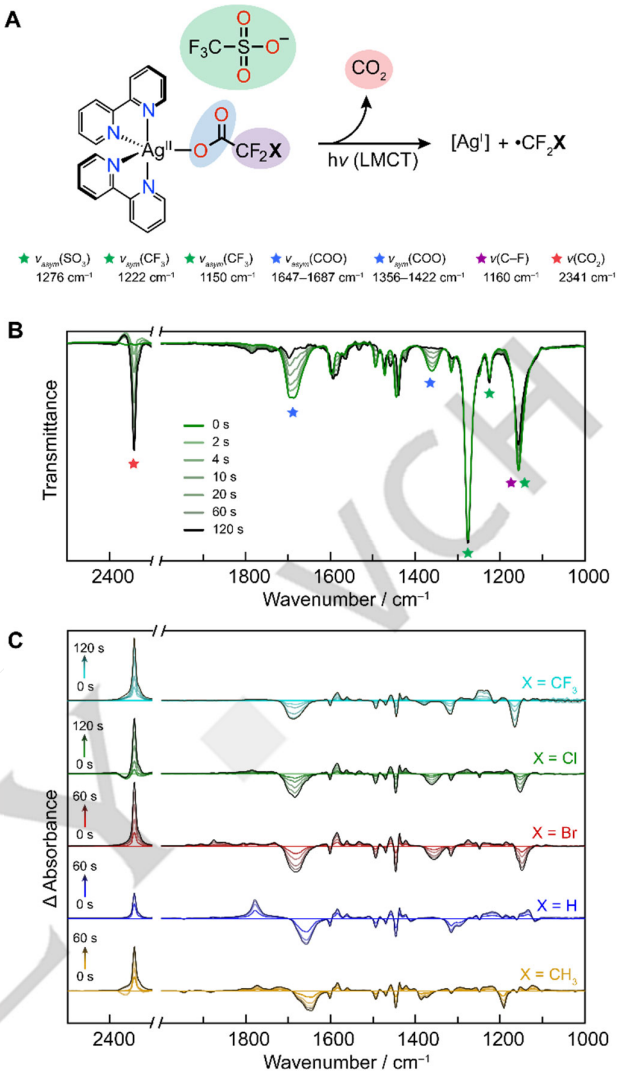

Figure 5. (**A**) Schematic of LMCT-induced decarboxylation of the [**1**–O_2CCF_2X][OTf] complexes. IR-active functional groups of interest are indicated by color (green: triflate; blue: carboxyl; purple: CF_2X; red: CO_2). (**B**) Steady-state FT-IR spectral evolution of a solution of [**1**–O_2CCF_2Cl][OTf] (5 mM, CD_3CN) under irradiation (λ_{exc} = 440 nm). Assigned IR stretches are labeled with the color-coded stars shown in (**A**). (**C**) Steady-state FT-IR difference spectra for solutions (5 mM, CD_3CN) of [**1**–$O_2CCF_2CF_3][BF_4]$ (cyan lines), [**1**–O_2CCF_2Cl][OTf] (green lines), [**1**–O_2CCF_2Br][OTf] (red lines), [**1**–O_2CCF_2H][OTf] (blue lines), and [**1**–$O_2CCF_2CH_3$][OTf] (yellow lines) under irradiation (λ_{exc} = 440 nm).

that the $\bullet O_2CCF_2H$ radical formed from LMCT undergoes H-atom transfer (HAT) competitively with decarboxylation. Consistently, less CO_2 is observed following photolysis of [**1**–O_2CCF_2H][OTf] as compared to the other five-coordinate complexes (**Figure 5C**). The **2**–$(O_2CCF_2X)_2$ complexes exhibit similar FT-IR spectral changes upon photolysis (**Figures S45**–**S47**). However, for these complexes, the asymmetric carboxyl stretch does not bleach completely, consistent with the retention of one intact carboxylate following LMCT. The

sharpened asymmetric carboxyl stretch coincides with that of the trigonal planar Ag^+ complexes, Ag(bpy)(O_2CCF_2X) (**Figure S47**).

The formation of fluoroalkyl radicals (•CF_2X) and Ag(I) as primary photoproducts (**Figure 5A**) is reflected in complementary spectroscopies. The observed loss of axial EPR signals upon irradiation of [**1**–O_2CCF_2X]$^+$ and **2**–(O_2CCF_2X)$_2$ is consistent with the generation of diamagnetic Ag(I) (**Figures S48–S54**), which was further validated by NMR spectroscopy. While solutions of [**1**–O_2CCF_2X]$^+$ or **2**–(O_2CCF_2X)$_2$ are ^{1}H NMR silent, irradiation produces new aryl resonances attributable to bpy ligands (**Figures S55–S59**). Furthermore, the appearance of HCF_2X and CF_2X_2 (X = Cl, Br) in ^{19}F spectra (**Figures S60–S61**) are consistent with •CF_2X-derived products resulting from radical abstraction reactions.[57]

Figure 6A shows the UV-vis spectral changes of [**1**–O_2CCF_2Cl][OTf] upon irradiation with 450 nm light. Similar spectra for the remaining [**1**–O_2CCF_2X]$^+$ and **2**–(O_2CCF_2X)$_2$ complexes are shown in **Figures S65**–**S71**. Complete bleaching of the visible absorption bands (inset of **Figure 6A**) is observed following irradiation, consistent with the generation of the Ag(I) photoproduct. In the UV spectral region, a shoulder at ca. 345 nm (ε_{345} = 5000 M^{-1} cm^{-1}) bleaches to baseline and a peak at 292 nm (ε_{292} = 31000 M^{-1} cm^{-1}), attributed primarily to bpy π–π^* transitions, blue shifts and decreases in intensity. A similar ligand-centered transition at 244 nm (ε_{244} = 21000 M^{-1} cm^{-1}) also decreases in intensity with the concomitant growth of a new feature at 237 nm. Overall, four isosbestic points at 281, 260, 237, and 229 nm are observed during photolysis, suggesting clean conversion of [**1**–O_2CCF_2Cl][OTf] to the Ag(I) photoproduct. In contrast, [**1**–O_2CCF_2H][OTf] exhibits distinct photochemical reactivity from the rest of the [**1**–O_2CCF_2X]$^+$ series (**Figure S68**). At early time points, similar bleaching of all visible absorption features is observed while a band at 373 nm persists (**Figure S72A**). Upon continued irradiation, this feature steadily decreases with the rise of a new broad absorption band extending from ca. 600–850 nm, with an isosbestic point at 411 nm (**Figure S72B**). Attempts to isolate this photoproduct were unsuccessful. While the **2**–(O_2CCF_2X)$_2$ complexes behave similarly to the five-coordinate complexes, early time points are characterized by the growth of the spectral feature at 700 nm before subsequent decay of this feature at later time points (**Figures S70–S71**), indicating transient formation of [**1**–O_2CCF_2X]$^+$ during photolysis. Though the above photochemical studies show that both the 5- and 4-coordinate complexes undergo LMCT reactivity with visible light to produce •CF_2X, under catalytic conditions (*vide infra*), when an excess of carboxylate is present, **2**–(O_2CCF_2X)$_2$ complexes are likely the major Ag(II) photoreagents in solution as showcased by the UV-vis titration data (**Figures S21–S24**). Further insight into the photochemistry of the Ag(II) complexes was provided by time-resolved femtosecond absorption spectroscopy. The extremely short-lived excited-state lifetime measured for **1**[OTf]$_2$ (τ < 20 ps) indicates that the carboxylate

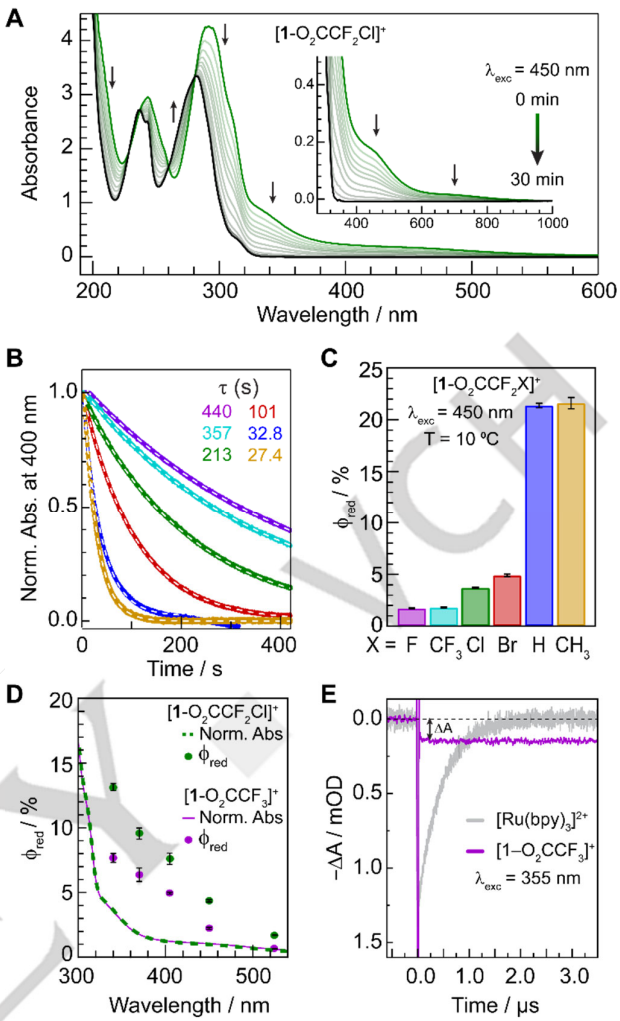

Figure 6. (**A**) Steady-state irradiation (λ_{exc} = 450 nm) of [**1**–O_2CCF_2Cl][OTf] (0.13 mM, CH_3CN) at 23 °C. Spectra were recorded at the following intervals: 0, 1, 2, 3, 4, 5, 7.5, 10, 15, 20, 30 min. Inset shows an expanded visible region of the UV-vis spectrum. (**B**) Absorbance vs time plots for the decay of solutions (ca. 0.1 mM, CH_3CN) of [**1**–O_2CCF_3][OTf] (purple), [**1**–$O_2CCF_2CF_3$][BF_4] (cyan), [**1**–O_2CCF_2Cl][OTf] (green), [**1**–O_2CCF_2Br][OTf] (red), [**1**–O_2CCF_2H][OTf] (blue), and [**1**–$O_2CCF_2CH_3$][OTf] (yellow) under irradiation (λ_{exc} = 450 nm, power = ca. 50 mJ/s) at 10 °C. (**C**) Photoreduction quantum yield of [**1**–O_2CCF_2X]$^+$ at λ_{exc} = 440 nm at 10 °C. Error bars represent the standard deviation of experiments performed in triplicate. (**D**) Action spectra of [**1**–O_2CCF_3][OTf] and [**1**–O_2CCF_2Cl][OTf] at 23 °C; quantum yields for [**1**–O_2CCF_3][OTf] (purple circles) and [**1**–O_2CCF_2Cl][OTf] (green circles) are superimposed on the normalized UV-vis spectrum of [**1**–O_2CCF_3I][OTf] (purple line) and [**1**–O_2CCF_2Cl][OTf] (green dashed line). (**E**) Overlay of the transient absorption kinetics of $[Ru(bpy)_2]^{2+}$ in H_2O at 490 nm (gray trace) as a reference, as well as [**1**–O_2CCF_3][OTf] (purple trace) in CH_3CN at 400 nm. The TA kinetics of [**1**–O_2CCF_3][OTf] were smoothed by adjacent averaging over 25 points. Per pulse energy = 60 μJ.

Single wavelength			Action spectra		
X	E_p (V)	Φ_{red} (%), 450 nm, 10 °C	λ_{exc}/nm	Φ_{red} (%), 23 °C	
				X = F	X = Cl
F	1.79	1.72 ± .05			
CF_3	1.71	1.81 ± 0.07	340	7.67 ± 0.35	13.14 ± 0.28
Cl	1.60	3.72 ± 0.04	370	6.38 ± 0.52	9.54 ± 0.09
Br	1.57	4.90 ± 0.14	405	4.94 ± 0.07	8.02 ± 0.43
H	1.28	21.37 ± 0.21	450	2.22 ± 0.09	4.36 ± 0.09
CH_3	1.20	21.62 ± 0.55	525	0.66 ± 0.02	1.71 ± 0.02

Table 1. Steady state photoreduction quantum yields (ϕ_{red}): (left) at 450 nm and 10 ºC, compared to the peak oxidation potential for [Na][O_2CCF_2X] (E_p, V vs Fc^+/Fc) for the [**1**–O_2CCF_2X]$^+$ series (right) at various excitation wavelengths for [**1**–O_2CCF_3]$^+$ and [**1**–O_2CCF_2Cl]$^+$ at 23 ºC (right side). Error represents the standard deviation of experiments performed in triplicate.

must be within the primary coordination sphere to undergo electron transfer (**Figure S73**).

The rates of [**1**–O_2CCF_2X]$^+$ photoreduction were measured upon 450-nm laser excitation by tracking the visible absorption decay over time; the photoreaction was performed at 10 °C to ensure thermal stability of the complexes (**Figure S25B**) during the course of photolysis. The observed lifetimes (τ) varied by an order of magnitude, with [**1**– $O_2CCF_2CH_3$][OTf] decaying at the fastest rate (τ = 27.4 s) and [**1**–O_2CCF_3][OTf] decaying the slowest (τ = 440 s) (**Figure 6B**). For [**1**–O_2CCF_2H][OTf], irradiation was constrained to early time points in which the visible absorption contributions from the unknown photoproducts are minimized.

Photoreduction quantum yields (ϕ_{red}) were calculated from the observed lifetimes following previously reported methods (Supporting Information, Section G).[58] Due to the thermal instability and complicated speciation of the **2**–$(O_2CCF_2X)_2$ complexes, quantification of their quantum yields was not undertaken. **Table 1** tabulates the measured quantum yields at a single wavelength for the [Na][O_2CCF_2X] complexes alongside the peak oxidation potentials (E_p) of their associated carboxylate ligand as well as action spectral data for for [**1**–O_2CCF_3]$^+$ and [**1**–O_2CCF_2Cl]$^+$ complexes. The increase in ϕ_{red} across the series (F ~ CF_3 < Cl < Br << H ~ CH_3, **Figure 6C**) is correlated with the oxidation potentials of the carboxylate ligands (**Figure 4B**), with ϕ_{red} increasing as the carboxylate ligand becomes easier to oxidize. The jump in ϕ_{red} between X = Br and X = H is reflected in the large difference in oxidation potential between [Na][O_2CCF_2Br] and [Na][O_2CCF_2H] (ΔE_{ox} = ca. 200 mV). To investigate how ϕ_{red} changes with irradiation wavelength, action spectra were collected at room temperature for both [**1**–O_2CCF_3][OTf] and [**1**–O_2CCF_2Cl][OTf]. For both complexes, the action spectra show an increase in ϕ_{red} from 525 nm to 340 nm (**Figure 6D**); we note a modest temperature dependence on ϕ_{red} is observed between 10 and 23 °C measurements (**Figure S94**). For [**1**–O_2CCF_3][OTf], ϕ_{red} appears to level off near 340 nm, as we previously observed,[29] whereas ϕ_{red} for [**1**–O_2CCF_2Cl][OTf] shows no signs of leveling. Attempts to measure ϕ_{red} at λ < 340 were not possible due to competitive absorption of photogenerated Ag(I) products. ϕ_{red} was also measured for [**1**–O_2CCF_3][OTf] at λ_{exc} = 355 nm using nanosecond transient absorption spectroscopy with $[Ru(bpy)_3]^{2+}$ as a reference (Supporting Information, Section G).[59,60] A persistent bleach allows for a ϕ_{red} determination of ca. 8% (**Figure 6E**), in agreement with the steady state data The bleach signal persists for >3 µs without recovery, indicating that parasitic processes on ϕ_{red}, such as back electron transfer, occur on a faster timescale than ca. 20 ns.

The high ϕ_{red} values reported here are significant, as quantum yields have been recognized as a determinant factor in the energy costs of photoredox methods.[46] Notably, appreciable quantum yields are maintained even with lower energy green light. These high photoreduction quantum yields, in both the visible and UV spectral regions, likely contribute to the fast reaction times observed for the Ag(II)–O_2CCF_2X complexes compared to related methods involving LMCT. Notwithstanding, the observed quantum yields only measure the efficiency of charge transfer from bound fluoroalkyl carboxylates to Ag(II). Subsequent steps important for fluoroalkylation reactivity, such as •CF_2X radical addition rates, can vary across the X series with trends differing from that observed for LMCT quantum efficiency. To probe the efficiency of these subsequent chemical steps, we undertook stoichiometric fluoroalkylation experiments using the isolated [**1**–O_2CCF_2X][OTf] complexes.

In the presence of excess benzene, [**1**–O_2CCF_2Cl][OTf] is rapidly consumed (20 min) under 440 nm irradiation, yielding (chlorodifluoromethyl)benzene in 45% yield (based on 1 equiv Ag), which is close to the theoretical maximum of 50% yield for this stoichiometric reaction, as 1 equiv of Ag(II) is needed to re-aromatize the ring (**Figure S95A**). The only other observed product by ^{19}F NMR spectroscopy is (H)O_2CCF_2Cl. In the absence of light, a 10% yield of (chlorodifluoromethyl)benzene is obtained after 20 h of heating at 60 °C, and degradation of the carboxylate to unidentified side products is observed (**Figure S95B**). Similarly, efficient production of (bromodifluoromethyl)-benzene is only observed under illumination conditions, in which 37% yield was achieved during 20 min of irradiation (λ_{exc} = 440 nm) with minimal byproducts (4% CF_2Br_2). If the reaction mixture is instead heated in the dark (60 °C, 18 h), only trace (bromodifluoromethyl)-benzene is produced (**Figure S96**). In contrast to [**1**–O_2CCF_2X][OTf] (X = Cl, Br), only trace amounts of benzene functionalization by CF_2X is observed upon irradiation of [**1**–O_2CCF_2H][OTf] or [**1**–$O_2CCF_2CH_3$][OTf] despite the higher ϕ_{red} values for these complexes (**Figures S97**–**S98**). It is known that the nucleophilic •CF_2H radical does not add efficiently to benzene,[61] as radical polarity is known to play a significant role in dictating the kinetics of radical addition.[62] Therefore, we attempted CF_2X (X = H, CH_3) functionalization of the more

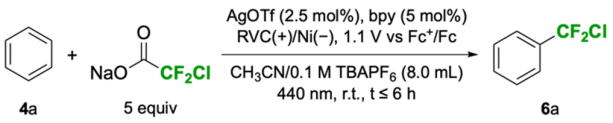

4a 5 equiv 6a

Entry	Deviation from optimal conditions	Yield (%)
1	None	57 = 49 mono + 8 bis
2	Constant current: 7.5 mA	50 = 45 mono + 5 bis
3	No Ag	0
4	No bpy	0
5	No light	0
6	$Cu(OTf)_2$ instead of AgOTf	0

Table 2. Reactions were performed in a divided, three-electrode electrochemical cell with benzene (**4a**, 0.5 mmol) as the limiting reagent. Yields were determined by ^{19}F NMR spectroscopy of the crude reaction mixtures, using $PhOCF_3$ as the internal standard. Constant potential reactions were halted at 6 h or when the measured current dropped to less than 1 mA. Constant current reactions were halted when a sharp increase in potential was observed.

electron-deficient substrate 1-methylquinoxalin-2(1H)-one, given the nucleophilicity of the $•CF_2H$ and $•CF_2CH_3$ radicals. Small quantities of the CF_2X-functionalized product were observed for X = H (5%, **Figure S99**) with higher quantities obtained for X = CH_3 (18%, **Figure S100**). Competing decomposition pathways likely contribute to the low yields of arene difluoromethylation (vide supra). Notably, a significant amount of difluoroacetic acid is observed following the LMCT of [**1**–O_2CCF_2H][OTf], suggesting that either the relative rate of HAT of the CF_2H carboxyl radical is faster than the other fluoroalkyl carboxyl radicals studied here, or its decarboxylation rate is slower. While [**1**–$O_2CCF_2CH_3$][OTf] possess the highest ϕ_{red}, it is also the most thermally unstable (*vide supra*), suggesting that low difluoroethylation yields may be observed due to competing thermal degradation pathways intrinsic to the Ag(II)–$O_2CCF_2CH_3$ complexes. This observation is consistent with the lack of chloro- and bromo-difluoromethylation when complexes [**1**–O_2CCF_2Cl][OTf] and [**1**–O_2CCF_2Br][OTf] are heated in the presence of benzene (**Figures S95–S96**).

Electrophotocatalysis

Building upon the observed photochemical behavior and stoichiometric fluoroalkylation reactivity of the [**1**–O_2CCF_2X][OTf] complexes, the scope of Ag(II)-mediated fluoroalkylation under catalytic conditions was explored by performing the photolyses under an applied potential in a divided electrochemical cell to electrochemically oxidize the Ag(I) photoproduct to regenerate Ag(II). We sought to improve upon the reaction conditions utilized for X = F and X = CF_3 in our previous report.[29] Starting from simple Ag(I) salts instead of the preformed **1**$[OTf]_2$, as well as utilizing lower ligand loadings and carboxylate equivalents (**Table S4**), the electrophotocatalytic chlorodifluoromethylation of benzene proceeded in moderate yields with turnover numbers exceeding 20 (**Table 2, entry 1**). Under this improved

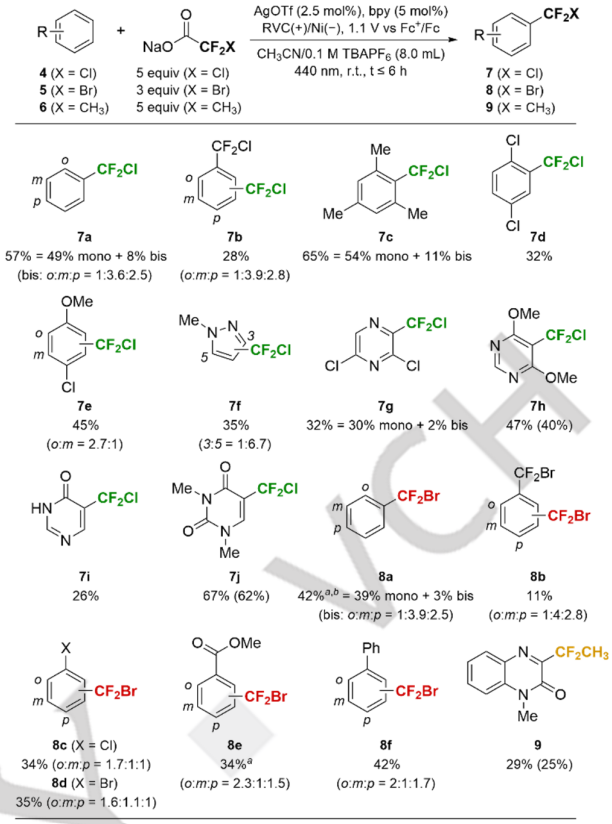

Table 3. Reactions were performed in a divided, three-electrode electrochemical cell with arene (**4**, **5**, or **6**, 0.5 mmol) as the limiting reagent. Yields were determined by ^{19}F NMR spectroscopy of the crude reaction mixtures, using $PhOCF_3$ or $PhCF_3$ as the internal standard. Isolated yields for non-volatile products are given in parentheses. Reactions were halted at 6 h or when the measured current dropped to less than 1 mA. Legend: [a]1.3 V vs Fc^+/Fc. [b]Carboxylate (10 equiv). r.t. = room temperature with fan cooling.

condition, the trifluoromethylation (58% = 53% mono + 5% bis) and pentafluoroethylation (83% = 72% mono + 11% bis) of benzene also proceeded in good yield. Constant current electrolyses could also be performed and afforded product in slightly diminished yield (**entry 2**). Control experiments indicated that light, bpy, and Ag(I) were all required for productive reactivity (**Entries 3–5**). When AgOTf was substituted with $Cu(OTf)_2$, no product was detected (**Entry 6**). This lack of reactivity is not due to an inability to form fluoroalkyl-carboxylate-ligated Cu complexes, as several of these complexes were isolated and crystallographically characterized (**Figures S12–S13**). Rather, the photoredox chemistry is obviated by the absence of accessible LMCT bands in the visible region (**Figure 2A**), consistent with the weaker oxidizing power of Cu(II) as compared to Ag(II).

Chloro- and bromodifluoromethylation, as well as difluoroethylation, may be extended beyond benzene to include other arenes, including pharmaceutically relevant heteroarenes (**Table 3**). A pyrazole substructure (**4f**), which is among the most common five-membered heteroarenes in

FDA-approved pharmaceuticals,[63–65] was efficiently chlorodifluoromethylated, predominantly at the 5-position. Medicinally prevalent six-membered heteroarenes, including pyrazine (**4g**), pyrimidine (**4h**), pyrimidone (**4i**), and uracil (**4j**) and quinoxalone (**6**) were also functionalized effectively. A variety of functional groups were accommodated, including aryl halides (**4d**–**e**, **4g**, **5c**–**d**), fluoroalkyl halides (**4b**, **5b**), and N–H heterocycles (**4i**). Additionally, despite the potential for H-atom abstraction at benzylic positions under radical reaction conditions, benzylic protons (**4c**) were well-tolerated. The radical reaction mechanism resulted in the formation of multiple regioisomers or difunctionalized products from some substrates, most of which could be chromatographically separated. For substrates of lower yields, we note that there are currently few options to synthesize these products, reflecting the difficulty associated with these reactions. Indeed, for many of these CF_2X functionalized (hetero)arenes, this is the first report of their synthesis and comprehensive characterization (e.g., ortho-7b, meta-7b, bis-7c, 5-7f, ortho-7e, 7g, bis-7g, 7h, 7i, ortho-8b, meta-8b, meta-8c, ortho-8d, ortho-8f, meta-8f).

Conclusion

Fluoroalkyl carboxylates are a widely available and general source of fluoroalkyl radicals, and the results presented here indicate that these ideal CF_2X sources can be activated by Ag(II) complexes. A series of bipyridyl Ag(II)–O_2CCF_2X (X = F, CF_3, Cl, Br, H, CH_3) complexes undergo LMCT photoreactivity under visible light irradiation, leading to decarboxylation of the ligated $^{-}O_2CCF_2X$ anion to liberate CO_2 and $\bullet CF_2X$ radicals, allowing for the straightforward installation of the CF_2X group via $C(sp^2)$–$C(sp^3)$ bond formation. The isolable nature of these complexes permits the study of how the quantum efficiency of bond homolysis systematically varies as a function of ligand identity. We find that the LMCT quantum yields scale with ligand oxidation potential. With the ability to tune the electronic properties of well-defined Ag(II) complexes, we anticipate that they will continue to find further use as LMCT photocatalysts for the activation of redox-reticent substrates.

Supporting Information

Materials and methods, synthetic procedures, crystallographic data, UV-vis, EPR, FT-IR, quantum yield data, and NMR spectra. The authors have cited additional references within the Supporting Information.[63–81]

Acknowledgements

This research was initially supported by the National Institutes of Health Grant GM047274 before the abrupt termination of the grant by the U.S. government. We thank Harvard University for its support, to allow this work to be completed. The authors would like to thank Dr. Shao-Liang Zheng for assistance with the SCXRD analysis of **2**–$(O_2CCF_2Cl)_2$ and **2**–$(O_2CCF_2Br)_2$, and Dr. Dongtao Cui for assistance with NMR experiments. We also thank Dr. David Gygi for helpful discussions. We acknowledge support of the X-ray core facility in the Department of Chemistry and Chemical Biology at Harvard University from the Major Research Instrumentation (MRI) Program of the National Science Foundation (NSF) under Award Numbers 2216066. BMC and MGS acknowledge support from the National Science Foundation Graduate Research Fellowship Program under Grant DGE-2140743 until these fellowships were too terminated. BMC also acknowledges support from the Herchel Smith Graduate Fellowship Program at Harvard University. JBG and ERR acknowledge support from NIH Postdoctoral Fellowships under Grant. No. F32GM147975 (JBG) and Grant No. F32GM153089 (ERR), which were also terminated.

Keywords: electrophotocatalysis • photochemistry • Ag(II) • radical reactions • fluoroalkylation

Entry for the Table of Contents

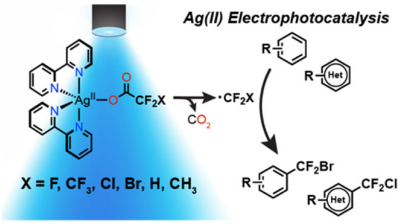

Fluoroalkylation methods beyond CF_3 incorporation are less common, but highly desirable. Herein, we leverage Ag(II) ligand-to-metal charge transfer (LMCT) to achieve catalytic installation of CF_2X moieties onto (hetero)arenes directly from abundant fluoroalkyl carboxylates. Furthermore, the isolation of a series of well-defined Ag(II) CF_2X carboxylate compounds allows for the study of how LMCT quantum efficiency is modulated by the X substituent.

References

[1] E. P. Gillis, K. J. Eastman, M. D. Hill, D. J. Donnelly, N. A. Meanwell, "Applications of Fluoride in Medicinal Chemistry." *J. Med. Chem.* **2015**, *58*, 8315–8359.

[2] K. Müller, C. Faeh, F. Diedrerich, "Fluorine in Pharmaceuticals: Looking Beyond Intuition." *Science* **2007**, *317*, 1881–1886.

[3] M. Inoue, Y. Sumii, N. Shibata, "Contribution of Organofluorine Compounds to Pharmaceuticals." *ACS Omega* **2020**, *5*, 10633–10640.

[4] K. L. Kirk, "Fluorination in Medicinal Chemistry: Methods, Strategies, and Recent Developments." *Org. Process. Res. Dev.* **2008**, *12*, 305–321.

[5] O. A. Tomashenko, V. V. Grushin, "Aromatic Trifluoromethylation with Metal Complexes." *Chem. Rev.* **2011**, *111*, 4475–4521.

[6] J. Charpentier, N. Früh, A. Togni, "Electrophilic Trifluoromethylation by Use of Hypervalent Iodine Reagents." *Chem. Rev.* **2015**, *115*, 650–682.

[7] S. Vaas, M. O. Zimmermann, D. Schollmeyer, J. Stahlecker, M. U. Engelhardt, J. Rheinganz, B. Drotleff, M. Olfert, M. Lämmerhofer, M. Kramer, T. Stehle, F. M. Boeckler, "Principles and Applications of CF_2X Moieties as Unconventional Halogen Bond Donors in Medicinal Chemistry, Chemical Biology, and Drug Discovery." *J. Med. Chem.* **2023**, *66*, 10202–10225.

[8] J. Gonzalez, C. J. Foti, S. Elsheimer, "Difluoromethylation of Alkenes via Borohydride Reduction of 1,3-Dibromo-1,1-Difluoroalkanes." *J. Org. Chem.* **1991**, *56*, 4322–4325.

[9] R. C. McAtee, J. W. Beatty, C. C. McAtee, C. R. J. Stephenson, "Radical Chlorodifluoromethylation: Providing a Motif for (Hetero)Arene Diversification." *Org. Lett.* **2018**, *20*, 3491–3495.

[10] N. A. Meanwell, "Synopsis of Some Recent Tactical Application of Bioisosteres in Drug Design." *J. Med. Chem.* **2011**, *54*, 2529–2591.

[11] A. Dorian, E. J. Landgreen, H. R. Petras, J. J. Shepherd, F. J. Williams, "Iron-Catalyzed Halogen Exchange of Trifluoromethyl Arenes." *Chem. Eur. J.* **2021**, *27*, 10839–10843.

[12] E. McBee, H. Hass, E. Hodnett, "Fluorinated Heterocyclic Compounds – Methylpyridines." *Ind. Eng. Chem.* **1947**, *39*, 389-391.

[13] E. Klauke, L. Oehlmann, B. Baasner, "Fluoronated Heterocyclic Compounds: Selective Chlorine/Fluorine Exchange Reactions on Pyridazines." *J. Fluor. Chem.* **1983**, *23*, 301–308.

[14] G. K. Surya Prakash, J. Hu, J. Simon, D. R. Bellew, G. A. Olah, "Preparation of α,α-Difluoroalkanesulfonic Acids." *J. Fluor. Chem.* **2004**, *125*, 595–601.

[15] S. A. Fuqua, R. M. Parkhurst, R. M. Silverstein, "Synthesis and Chemistry of Several Fluorinated *p*-Xylenes Designed as Precursors for α,α,α´,α´-Tetrafluoro-*p*-xylylene." *Tetrahedron* **1964**, *20*, 1625–1632.

[16] J. P. Chupp, J. M. Molyneaux, "Derivation of Fluorine-Containing Pyridinedicarboxylates. III Regioselective Anion Chemistry at the 2- and 4-Position." *J. Heterocyclic Chem.* **1989**, *26*, 1771–1780.

[17] D. Mandal, R. Gupta, A. K. Jaiswal, R. D. Young, "Frustrated Lewis-Pair-Mediated Selective Single Fluoride Substitution in Trifluoromethyl Groups." *J. Am. Chem. Soc.* **2020**, *142*, 2572–2578.

[18] A. L. Trifonov, A. D. Dilman, "Synthesis of Difluoroalkylated Heteroarenes via Difluorocarbene." *Org. Lett.* **2021**, *23*, 6977–6981.

[19] R. Y. Yang, X. Gao, K. Gong, J. Wang, X. Zeng, M. Wang, J. Han, B. Xu, "Synthesis of $ArCF_2X$ and [^{18}F]Ar–CF_3 via Cleavage of the Trifluoromethylsulfonyl Group." *Org. Lett.* **2022**, *24*, 164–168.

[20] B. H. Luo, H. P. Guan, C. M. Hu, "One Pot Synthesis of Fluoroalkyl Pyrimidines from α-Fluoroalkyl Carbonyl Compounds, Orthoesters, and Ammonium Carbonate." *Synlett,* **1997**, *11*, 1261–1262.

[21] V. O. Iaroshenko, V. Specowius, K. Vlach, M. Vilches-Herrera, D. Ostrovskyi, S. Mkrtchyan, A. Villinger, P. A. Langer, "General Strategy for the Synthesis of Difluoromethyl-Containing Pyrazoles, Pyridines and Pyrimidines." *Tetrahedron* **2011**, *67*, 5663–5677.

[22] H. Jiang, S. Yuan, Y. Cai, W. Wan, S. Zhu, J. Hao, A Facile "Preparation of 2-Bromodifluoromethyl Benzo-1,3-Diazoles and its Application in the Synthesis of *gem*-Difluoromethylene Linked Aryl Ether Compounds." *J. Fluor. Chem.* **2012**, *133*, 167–170.

[23] B. Duda, S. N. Tverdomed, B. I. Ionin, G. V. Röschenthaler, "Fluorinated Alkynlphosphonates in *C,C*-Cyclizations: Regioselective Formation of Polysubstituted Fluorinated Arylphosphonates." *Eur. J. Org. Chem.* **2014**, *2014*, 3757–3761.

[24] S. Kawamura, C. J. Henderson, Y. Aoki, D. Sekine, S. Kobayashi, M. Sodeoka, "Reactivity and Properties of bis(Chlorodifluoroacetyl) Peroxide Generated *in situ* from Chlorodifluoroacetic Anhydride for Chlorodifluoromethylation Reactions." *Chem. Commun.* **2018**, *54*, 11276–11279.

[25] D. Lin, V. Krishnamurti, G. K. Surya Prakash, "Visible Light-Mediated Metal-Free Chlorodifluoromethylation of Arenes and Heteroarenes by a Hypervalent Iodine EDA Complex." *Eur. J. Org. Chem.* **2022**, *2022*, e202200607.

[26] Q. W. Gui, F. Teng, H. Yang, C. Xun, W. J. Huang, Z. Q. Lu, M. X. Zhu, W. T. Ouyang, W. M. He, "Visible-Light Photosynthesis of CHF_2/$CClF_2$/$CBrF_2$-Substituted Ring-Fused Quinazolinones in Dimethyl Carbonate." *Chem. Asian. J.* **2022**, *17*, e202101139.

[27] J. Qi, J. Xu, H. T. Ang, B. Wang, N. K. Gupta, S. R. Dubbaka, P. O'Neill, X. Mao, Y. Lum, J. Wu, "Electrophotochemical Synthesis Facilitated Trifluoromethylation of Arenes Using Trifluoroacetic Acid." *J. Am. Chem. Soc.* **2023**, *145*, 24965–24971.

[28] C. Depecker, H. Marzouk, S. Trevin, J. Devynck, "Trifluoromethylation of Aromatic Compounds *via* Kolbe Electrolysis in Pure Organic Solvent. Study on Laboratory and Pilot Scale." *New J. Chem.* **1999**, *23*, 739–742.

[29] B. M. Campbell, J. B. Gordon, E. R. Raguram, M. I. Gonzalez, K. G. Reynolds, M. Nava, D. G. Nocera, "Electrophotocatalytic Perfluoroalkylation by LMCT Excitation of Ag(II) Perfluoroalkyl Carboxylates." *Science* **2024**, *383*, 279–284.

[30] K. J. Bian, Y. C. Lu, D. Nemoto, S. C. Kao, X. Chen, J. G. West, "Photocatalytic Hydrofluoroalkylation of Alkenes with Carboxylic Acids. *Nat. Chem.* **2023**, *15*, 1683–1692.

[31] S. Fernández-García, V. O. Chantzakou, F. Juliá-Hernández, "Direct Decarboxylation of Trifluoroacetates Enabled by Iron Photocatalysis." *Angew. Chem. Int. Ed.* **2024**, *63*, e202311984.

[32] Q. Zhu, D. G. Nocera, "Photocatalytic Hydromethylation and Hydroalkylation of Olefins Enabled by Titanium Dioxide Mediated Decarboxylation." *J. Am. Chem. Soc.* **2020**, *142*, 17913–17918.

[33] V. Motornov, S. Trienes, S. Resta, J. C. A. Oliveira, Z. Lin, Z. Liu, T. von Münchow, C. Stückl, L. Ackermann, "Photoelectrochemical Iron(III) Catalysis for Late-Stage C–H Fluoroalkylations." *Angew. Chem. Int. Ed.* **2025**, e202504143.

[34] R. Fayad, S. Engl, E. O. Danilov, C. E. Hauke, O. Reiser, F. N. Castellano, "Direct Evidence of visible Light-Induced Homolysis in Chlorobis(2,9-Dimethyl-1,10-Phenanthroline)Copper(II)." *J. Phys. Chem. Lett.* **2020**, *11*, 5345–5349.

[35] Q. Y. Li, S. N. Gockel, G. A. Lutovsky, K. S. DeGlopper, N. J. Baldwin, M. W. Bundesmann, J. W. Tucker, S. W. Bagley, T. P. Yoon, "Decarboxylative Cross-Nucleophile Coupling via Ligand-to-Metal Charge Transfer Photoexcitation of Cu(II) Carboxylates." *Nat. Chem.* **2022**, *14*, 94–99.

[36] W. Su, P. Xu, R. Petzold, J. Yan, T. Ritter, "Ligand-to-Copper Charge-Transfer-Enabled C–H Sulfoximination of Arenes." *Org. Lett.* **2023**, *25*, 1025–1029.

[37] M. I. Gonzalez, D. Gygi, Y. Qin, Q. Zhu, E. J. Johnson, Y-S. Chen, D. G. Nocera, "Taming the Chlorine Radical: Enforcing Steric Control Over Chlorine-Radical-Mediated C–H Activation." *J. Am. Chem. Soc.* **2022**, *144*, 1464–1472.

[38] H. Guo, W. Lai, J. Ni, P. Xu, "Synthesis of Alkyl bis(Trifluoromethyl)Carbinols via Fe-LMCT-Enabled

Hydrobis(trifluoromethyl)carbinolation of Alkenes." *Org. Lett.* **2024**, *26*, 9568–9573.

[39] Q. An, Z. Wang, Y. Chen, X. Wang, K. Zhang, H. Pan, W. Liu, Z. Zuo, "Cerium-Catalyzed C–H Functionalizations of Alkenes Utilizing Alcohols as Hydrogen Atom Transfer Agents." *J. Am. Chem. Soc.* **2020**, *142*, 6216–6226.

[40] S. J. Hwang, D. C. Powers, A. G. Maher, B. L. Anderson, R. G. Hadt, S. L. Zheng, Y. S. Chen, D. G. Nocera, "Trap-Free Halogen Photoelimination from Mononuclear Ni(III) Complexes." *J. Am. Chem. Soc.* **2015**, *137*, 6472–6475.

[41] D. A. Cagan, D. Bím, B. Silva, N. P. Kazmierczak, B. J. McNicholas, R. G. Hadt, "Elucidating the Mechanism of Excited-State Bond Homolysis in Nickel-Bipyridine Photoredox Catalysts." *J. Am. Chem. Soc.* **2022**, *144*, 6516–6531.

[42] A. T. Barth, A. J. Pyrch, C. T. McCormick, E. O. Danilov, F. N. Castellano, "Excited State Bond Homolysis of Vandium(V) Photocatalysts for Alkoxy Radical Generation." *J. Phys. Chem. A* **2024**, *128*, 7609–7619.

[43] W. Han, Z. Zhao, K. Jiang, Y. Lan, X. Yu, X. Jiang, W. Yang, D. Wei, S. J. Li, L. Niu, "Dual Ligand-Enabled Iron and Halogen-Containing Carboxylate-Based Photocatalysis for Chloro/Fluoro-Polyhaloalkylation of Alkenes." *Chem. Sci.* **2024**, *15*, 19936–19943.

[44] Y. Qin, B. C. M. Martindale, R. Sun, A. J. Rieth, D. G. Nocera, "Solar-Driven Tandem Photoredox Nickel-Catalysed Cross-Coupling Using Modified Carbon Nitride." *Chem. Sci.* **2020**, *11*, 7456–7461.

[45] S. Ruccolo, Y. Qin, C. Schnedermann, D. G. Nocera, "General Strategy for Improving the Quantum Efficiency of Photoredox Hydroamidation Catalysis." *J. Am. Chem. Soc.* **2018**, *140*, 14926–14937.

[46] J. R. Swierk, "The Cost of Quantum Yield." *Org. Process Res. Dev.* **2023**, *27*, 1411–1419.

[47] J. Struwe, L. Ackermann, "Photoelectrocatalyzed Undirected C–H Trifluoromethylation of Arenes: Catalyst Evaluation and Scope." *Faraday Discuss.* **2023**, *247*, 79–86.

[48] Y. Qiu, A. Scheremetjew, L. H. Finger, L. Ackermann, "Electrophotocatalytic Undirected C–H Trifluoromethylations of (Het)Arenes." *Chem. Eur. J.* **2020**, *26*, 3241–3246.

[49] X.-L. Lai, X.-M. Shu, J. Song, H.-C. Xu, "Electrophotocatalytic Decarboxylative C–H Functionalization of Heteroarenes." *Angew. Chem. Int. Ed.* **2020**, *59*, 10626–10632.

[50] W. Grochala, Z. Mazej, "Chemistry of Silver(II): A Cornucopia of Peculiarities." *Phil. Trans. Royal Soc. A* **2015**, *373*, 20140179.

[51] Deposition numbers 2428197 (for [**1**–Cu–O2CCF$_2$Br][PF$_6$]), 2428198 (for [**1**–Cu–O2CCF$_2$Cl][PF$_6$]), 2428199 (for [**1**–O2CCF$_2$Br][OTf]), 2428200 (for [**1**–O2CCF$_2$CH$_3$][OTf]), 2428201 (for [**1**–O2CCF$_2$Cl][OTf]), 2428202 (for [**1**–O2CCF$_2$H][OTf]), 2428203 (for **2**–(O$_2$CCF$_2$Br)$_2$), 2428204 (for **2**–(O$_2$CCF$_2$CH$_3$)$_2$), 2428205 (for **2**–(O$_2$CCF$_2$Cl)$_2$), and 2445900 (for [**1**–O2CCF$_2$CF$_3$][BF$_4$]) contain the supplementary crystallographic data for this paper. These data are provided free of charge by the joint Cambridge Crystallographic Data Centre and Fachinformationszentrum Karlsruhe Access Structures service.

[52] A. W. Addison, T. N. Rao, J. Reedijk, J. van Rijn, G. C. Verschoor, "Synthesis, Structure, and Spectroscopic Properties of Copper(II) Compounds Containing Nitrogen-Sulphur Donor Ligands; the Crystal and Molecular Structure of Aqua[1,7-bis(*N*-Methylbenzimidazol-2′-yl)-2,6-Dithiaheptane]Copper(II) Perchlorate." *J. Chem. Soc. Dalton Trans,* **1984**, *7*, 1349-1356

[53] H. R. Pan, H. J. Chen, Z. H. Wu, P. Ge, S. Ye, G. H. Lee, H. F. Hsu, "Structural and Spectroscopic Evidence for a Side-on Fe(III)–Superoxo Complex Featuring Discrete O–O Bond Distances." *JACS Au* **2021**, *1*, 1389–1398.

[54] L. Yang, D. R. Powell, R. P. Houser, "Structural Variation in Copper(I) Complexes with Pyridylmethylamide Ligands: Structural Analysis with a New Four-Coordinate geometry Index." τ_4. *Dalton Trans.* **2007**, *9,* 955–964.

[55] A. B. P. Lever, "Charge Transfer Spectra of Transition Metal Complexes." *J. Chem. Ed.* **1974**, *51*, 612–616.

[56] T. Mairegger, H. Li, C. Grießer, D. Wrinkler, J. Filser, N. G. Hörmann, K. Reuter, J. Kunze-Liebhäuser, "Electroreduction of CO_2 in a Non-aqueous Electrolyte – The Generic Role of Acetonitrile." *ACS Catal.* **2023**, *13*, 5780–5786.

[57] P. S. Bhadury, M. Palit, M. Sharma, S. K. Raza, D. K. Jaiswal, "Fluorinated Phosphonium Ylides: Versatile *in situ* Wittig Intermediates in the Synthesis of Hydrofluorocarbons." *J. Fluor. Chem.* **2002**, *116*, 75–80.

[58] E. Stadler, A. Eibel, D. Fast, H. Freißmuth, C. Holly, M. Wiech, N. Moszner, G. Gescheidt, "A Versatile Method for the Determination of Photochemical Quantum Yields via Online UV-Vis Spectroscopy." *Photochem. Photobiol. Sci.* **2018**, *17*, 660–669.

[59] P. Müller, K. Brettel, "$[Ru(bpy)_3]^{2+}$ as a Reference in Transient Absorption Spectroscopy: Differential Absorption Coefficients for Formation of the Long-Lived ^{3}MLCT Excited State." *Photochem. Photobiol. Sci*. **2012**, *11*, 632–636.

[60] M. Byrdin, A. Lukacs, V. Thiagarajan, A. P. M. Eker, K. Brettel, M. H. Vos, "Quantum Yield Measurements of Short-Lived Photoactivation Intermediates in DNA Photolyase: Toward a Detailed Understanding of the Triple Tryptophan Electron Transfer Chain." *J. Phys. Chem. A* **2010**, *114*, 3207–3214.

[61] A. J. Fernandes, R. Giri, K. N. Houk, D. Katayev, "Review and Theoretical Analysis of Fluorinated Radicals in Direct CAr−H Functionalization of (Hetero)Arenes." *Angew. Chem. Int. Ed.* **2024**, *63*, e202318377.

[62] J. J. A. Garwood, A. D. Chen, D. A. Nagib, "Radical Polarity." *J. Am. Chem. Soc.* **2024**, *146*, 28034–28059.

[63] E. Vitaku, D. T. Smith, J. T. Njardarson, "Analysis of the Structural Diversity, Substitution Patterns, and Frequency of Nitrogen Heterocycles among U.S. FDA Approved Pharmaceuticals." *J. Med. Chem.* **2014**, *57*, 10257−10274.

[64] C. M. Marshall, J. G. Federice, C. N. Bell, P. B. Cox, J. T. Njardarson, "An Update on the Nitrogen Heterocycle Compositions and Properties of U.S. FDA-Approved Pharmaceuticals (2013−2023)." *J. Med. Chem.* **2024**, *67*, 11622−11655.

[65] R. D. Taylor, M. MacCoss, A. D. Lawson, "Rings in Drugs." *J. Med. Chem.* **2014**, *57*, 5845−5859.

SI Refs

[66] E. Szłyk, R. Szczęsny, A. Wojtczak, "X-ray Structural and Gas Phase Studies of Dilver(I) Perfluorinated Carboxylate Complexes with 2,2′-Bipyridal as Potential Precursors for Chemical Vapor Deposition (CVD)." *Dalton Trans.* **2010**, *39*, 1823–1830.

[67] S. Tyagi, B. Hathaway, S. Kremer, H. Stratemeier, D. Reinen, "Crystal Structure of Bis(2,2′-bipyridyl)monochlorocopper(II) Hexafluorophosphate Monohydrate at 298 K and the Electron Spin Resonance Spectra of Some Bis(2,2′-bipyridyl)copper(II) Complexes to 4.2 K." *J. Chem. Soc., Dalton Trans.* **1984**, 2087–2091.

[68] D. F. Evans, "400. The Determination of the Paramagnetic Susceptibility of Substances in Solution by Nuclear Magnetic Resonance." *J. Chem. Soc.* **1959**, 2003–2005.

[69] G. A. Bain, J. F. Berry, "Diamagnetic Corrections and Pascal's Constants." *J. Chem. Ed.* **2008**, *85*, 532–536.

[70] G. M. Sheldrick, CELL NOW V2008/2, Bruker AXS (2008).
[71] G. M. Sheldrick, TWINABS, Bruker Analytical X-ray Systems (2014).
[72] G. M. Sheldrick, SADABS, Bruker Analytical X-ray Systems (2014).
[73] G. M. Sheldrick, "SHELXT-Integrated Space-group and Crystal-Structure Determination." *Acta Crystallogr. A Found. Adv.* **2015**, *71*, 3–8.
[74] G. M. Sheldrick, SHELXL (University of Göttingen, 2014).
[75] O. V. Dolomanov, L. J. Bourhis, R. J. Gildea, J. A. K. Howard, H. Puschmann, "OLEX2: A Complete Structure Solution, Refinement and Analysis Program." *J. Appl. Cryst.* **2009**, *42*, 339–341.
[76] A. M. Mills, J. A. M. v. Beek, G. v. Koten, A. L. Spek, "{2,6-Bis[(dimethylamino-κN)methyl]phenyl-κC}iodopalladium(II) bis(diiodine)." *Acta Cryst. C*, **2002**, *58*, m304–m306.
[77] A. Foris, "^{19}F and ^{1}H NMR Spectra of Halocarbons." *Magn. Reson. Chem.* **2004**, *42*, 534–555.
[78] C. G. Hatchard, C. A. Parker, "A New Sensitive Chemical Actinometer - II. Potassium Ferrioxalate as a Standard Chemical Actinometer." *Proc. Royal Soc. London Ser. A* **1956**, *235*, 518–536.
[79] W. R. Dolbier, J-X. Duan, X. X. Rong, "Efficient Synthesis of p-Bis(chlorodifluoromethyl)benzene." *J. Fluor. Chem.* **2007**, *10*, 1091–1093.
[80] R. Idogawa, Y. Kim, K. Shimomori, T. Hosoya, S. Yoshida, "Single C–F Transformations of o-Hydrosilyl Benzotrifluorides with Trityl Compounds as All-In-One Reagents." *Org. Lett.* **2020**, *22*, 9292–9297.
[81] T. J. O'Connor, B. K. Mai, J. Nafie, P. Liu, F. D. Toste, "Generation of Axially Chiral Fluoroallenes through a Copper-Catalyzed Enantioselective β-Fluoride Elimination." *J. Am. Chem. Soc.* **2021**, *143*, 13759–13768.
[82] A. Haas, M. Spitzer, M. Lieb, "Synthese Seitenkettenfluorierter Aromatischer Verbindungen und deren Chemische Reaktivität." *Chem. Ber.* **1988**, *121*, 1329–1340.
[83] S. Verhoog, L. Pfeifer, T. Khotavivattana, S. Calderwood, T. L. Collier, K. Wheelhouse, M. Tredwell, V. Gouverneur, "Silver-Mediated ^{18}F-labeling of Aryl-CF_3 and Aryl-CHF_2 with ^{18}F-Fluoride." *Synlett* **2016**, *27*, 25–28.
[84] J. W. Gu, W. H. Guo, X. Zhang, "Synthesis of Diaryldifluoromethanes by Pd-Catalyzed Difluoroalkylation of Arylboronic Acids." *Org. Chem. Front.* **2015**, *2*, 38–41.
[85] G. Hong, J. Yuan, J. Fu, G. Pan, Z. Wang, L. Yang, Y. Xiao, P. Mao, X. Zhang, "Transition-Metal-Free Decarboxylative C_3-Difluoroarylmethylation of Quinoxalin-2(1H)-ones with α,α-Difluoroarylacetic Acids." *Org. Chem. Front.* **2019**, *6*, 1173–1182.